

HYDROGELS

Hydrogel-based strong and fast actuators by electroosmotic turgor pressure

Hyeonuk Na^{1†}, Yong-Woo Kang^{1†}, Chang Seo Park^{1†}, Sohyun Jung^{2†}, Ho-Young Kim^{2*}, Jeong-Yun Sun^{1,3*}

Hydrogels are promising as materials for soft actuators because of qualities such as softness, transparency, and responsiveness to stimuli. However, weak and slow actuations remain challenging as a result of low modulus and osmosis-driven slow water diffusion, respectively. We used turgor pressure and electroosmosis to realize a strong and fast hydrogel-based actuator. A turgor actuator fabricated with a gel confined by a selectively permeable membrane can retain a high osmotic pressure that drives gel swelling; thus, our actuator exerts large stress [0.73 megapascals (MPa) in 96 minutes (min)] with a 1.16 cubic centimeters of hydrogel. With the accelerated water transport caused by electroosmosis, the gel swells rapidly, enhancing the actuation speed (0.79 MPa in 9 min). Our strategies enable a soft hydrogel to break a brick and construct underwater structures within a few minutes.

Because of their softness, transparency, biocompatibility, and responsiveness to stimuli, hydrogels are attractive candidates for soft actuators and have been applied in various fields such as soft robotics (1, 2), tunable optics (3), fluidics (4), and biomedicine (5). The actuation mechanism of most hydrogel actuators is swelling, driven by osmotic pressure in response to external stimuli such as solvent (6), temperature (7), pH (8), electric field (9), and light (10). However, hydrogel soft actuators generally suffer from small actuation stress (i.e., actuation force per unit area) and low speed. The weak actuation stress comes from the low elastic modulus and strength of the hydrogel, whereas the low actuation speed is attributed to osmotic swelling, which proceeds with the diffusion of water.

Although the actuation stress of a hydrogel actuator is usually weak (i.e., 1 to 100 kilopascals), the osmotic pressure of the hydrogel—the origin of the actuation—is able to reach ~50 megapascals (MPa) (11). Previous studies on hydrogel actuators have not focused on converting the high osmotic pressure to a corresponding strong actuation stress. However, in nature, plant cells harness their high osmotic pressure to achieve strong turgor pressure. Turgor pressure is the hydrostatic pressure in plant cells resulting from the osmosis-driven swelling confined by the stiff semipermeable cell walls. The turgor pressure equalizes with the high osmotic pressure, allowing soft plant cells to support their bodies, dig deep into the soil, and even break solid rocks. Likewise, a system that uses turgor pressure is expected to

improve the actuation stresses of the hydrogel actuators by exploiting the high osmotic pressure.

Most hydrogel actuators suffer from low speeds due to their diffusion-based actuation mechanisms. Many studies have attempted to improve these actuation speeds by increasing diffusion rates or using different actuation mechanisms; these include the molecular engineering of stimuli-responsive hydrogels (12–15), the incorporation of active materials into hydrogel matrices (16), use of the elastic potential energy of the hydrogel network (17), and the pneumatic or hydraulic actuation of the hydrogel cover structure (18). Despite substantial improvements in speed, actuation forces have been limited to <1 N (19) because hydrogels are intrinsically soft. A mechanism that accelerates swelling is expected to create synergy with a system that can use turgor pressure and thus is promising in achieving both fast and strong actuations. Swelling can be accelerated by adopting a fast water-transport mechanism. Electroosmosis induces a constant and rapid water flow through a charged porous material under an electric field and can thus accelerate the swelling of hydrogels because the migrating ions drag the nearby water into the charged polymer network.

We report a hydrogel-based actuator with a design that uses turgor pressure and electroosmosis, which can achieve much higher actuation force in a shorter time than conventional hydrogel actuators. Wrapped in a membrane, a hydrogel converts its inherent high osmotic pressure to a large actuation stress. The actuation stress of a hydrogel actuator (bare) can be characterized by the blocking stress (σ_{block}) of a constrained swelling between two rigid plates at the equilibrium state (Fig. 1, A and B); the blocking stress can be predicted with the ideal elastomeric gel model (20). The model presents equations of state for a swollen hydrogel (Eqs. 1 and 2), which are used to determine the swelling stress (σ_{sw})—the stress that a hydrogel applies outward—on the basis

of the difference between two competing terms: (i) the water inflow pressure (P_{in}), which is the driving force for the volumetric expansion of a hydrogel and is equal to the osmotic pressure (π_{os}) in an aqueous environment ($P_{\text{in}} = \pi_{\text{os}}$); and (ii) the elastic stress (σ_{el}), which is the elastic restoring stress of the polymer network which prevents swelling

$$\sigma_{\text{sw},i} = P_{\text{in}} - \sigma_{\text{el},i} = \pi_{\text{os}} - \sigma_{\text{el},i} \quad (i = x, y, z) \quad (1)$$

$$\sigma_{\text{el},i} = \frac{NkT}{J} (\lambda_i^2 - 1) \quad (i = x, y, z) \quad (2)$$

where N is the number of polymer chains per unit volume of a dry network, and kT is the temperature in the unit of energy. π_{os} is a function of the swelling ratio (J) and has the same value regardless of the direction. $J = \lambda_x \lambda_y \lambda_z$, where λ_i is the stretch ratio from the initial hydrogel unit cube in the i direction.

A constrained swelling of a bare gel meets $\sigma_{\text{sw},x} = \sigma_{\text{sw},y} = 0$ and $\lambda_x = \lambda_y$ in the equilibrium state, as shown in Fig. 1A. From Eq. 1, $\pi_{\text{os}} = \sigma_{\text{el},x} = \sigma_{\text{el},y}$, and the blocking stress is calculated as

$$\begin{aligned} \sigma_{\text{block}}^{\text{bare}} &= \sigma_{\text{sw},z} = \pi_{\text{os}} - \sigma_{\text{el},z} \\ &= \sigma_{\text{el},x} - \sigma_{\text{el},z} = \frac{NkT}{J} (\lambda_x^2 - \lambda_z^2) \end{aligned} \quad (3)$$

where $NkT/J^{1/3}$ is the shear modulus of a gel, which is generally low (e.g., below 50 kPa) (20, 21), resulting in the weak blocking stress presented by bare hydrogels. The shear modulus of the fully swollen hydrogel used in our experiment was measured as 8.24 kPa with $J = 125$ (Fig. 1C); further, the blocking stress of the bare hydrogel was limited even below NkT , i.e., 41.2 kPa (see methods for details). At the equilibrium state, the remaining osmotic pressure is as low as its weak elastic stress, which leads to the weak blocking stress.

In our turgor actuator (Fig. 1B), which is a hydrogel wrapped in a selectively permeable and relatively stiff membrane, the membrane prevents the swelling of the gel. As a result, a high osmotic pressure can be retained in the hydrogel, thus causing the contribution of the polymer elastic stress (σ_{el}) to the swelling stress (σ_{sw}) to become negligible (Fig. 1C). Then, the swelling stress equals the osmotic pressure:

$$\begin{aligned} \sigma_{\text{sw},i} &= P_{\text{in}} - \sigma_{\text{el},i} = \pi_{\text{os}} - \sigma_{\text{el},i} \approx \\ &\pi_{\text{os}} \quad (i = x, y, z) \end{aligned} \quad (4)$$

Therefore, the gel inside the membrane can act similar to a liquid under a hydrostatic pressure equal to the osmotic pressure. In the transverse (x, y) direction, the swelling stress is balanced with the membrane pressure (P_{memb}) (see supplementary text and fig. S1).

$$P_{\text{memb}} \approx \pi_{\text{os}} \quad (5)$$

¹Department of Material Science and Engineering, Seoul National University, Seoul 08826, Republic of Korea.

²Department of Mechanical Engineering, Seoul National University, Seoul 08826, Republic of Korea. ³Research Institute of Advanced Materials (RIAM), Seoul National University, Seoul 08826, Republic of Korea.

*Corresponding author. Email: hyk@snu.ac.kr (H.-Y.K.); jysun@snu.ac.kr (J.-Y.S.)

†These authors contributed equally to this work.

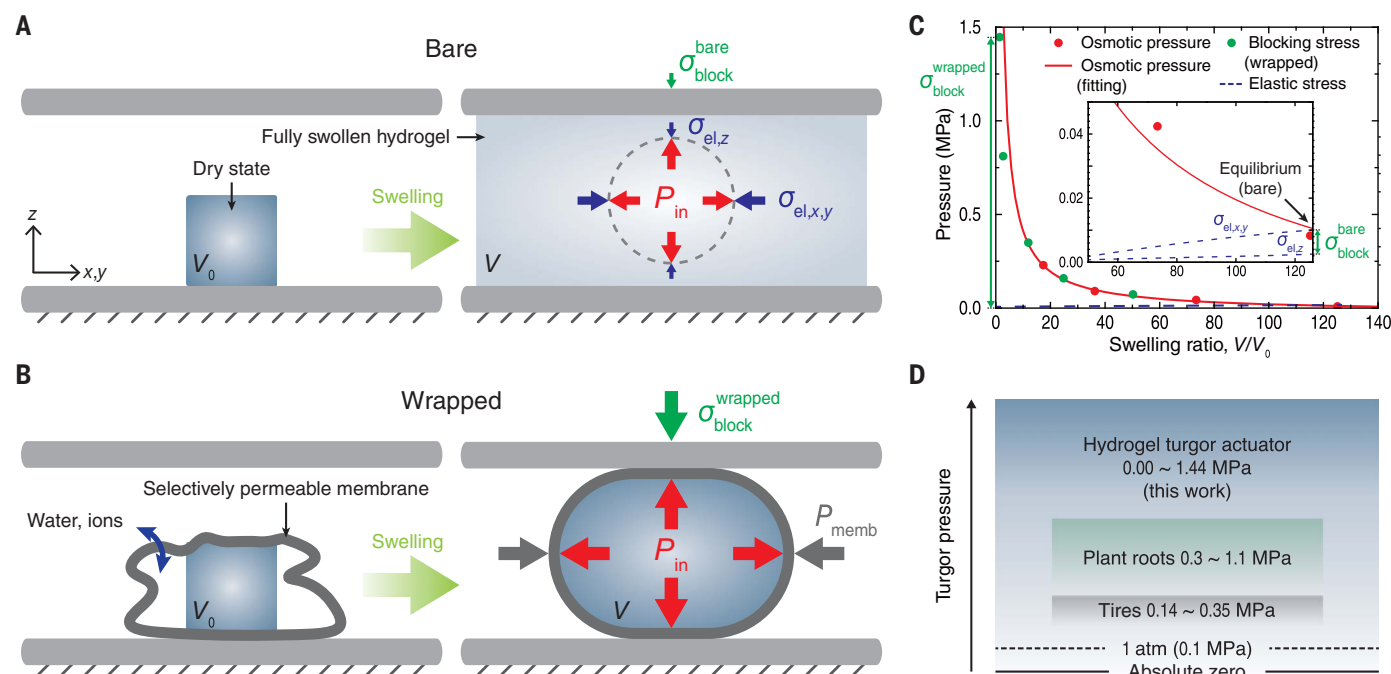


Fig. 1. Design and principle of a hydrogel turgor actuator. (A and B) Schematic illustrations of constrained osmotic swelling of hydrogel between two fixed plates (A) without membrane (bare) and (B) with membrane (wrapped). The initial hydrogel is a dry polymer cube with a volume of V_0 . V , volume of the hydrogel after swelling. Pressure and stress within the gels are represented as colored arrows; red is water inflow pressure (P_{in}), and blue is elastic stress (σ_{el}). The membrane stress (σ_{memb}) in the membrane cross section is represented by dark gray arrows and the blocking stress (σ_{block}) is represented by green arrows. When the hydrogel swells in a membrane by osmosis, the water inflow pressure becomes the osmotic pressure of the gel $P_{in} = \pi_{os}$, and the high osmotic pressure can be sustained by the turgor pressure originating

from the membrane tension leading to the generation of a large blocking stress. (C) The osmotic pressure and the elastic stress developed in PSPA hydrogel as a function of the swelling ratio (V/V_0). The osmotic pressure of the gel (red dot and line) was measured by dynamic mechanical analysis. The blocking stresses of the hydrogel turgor actuators (green dot) were measured by a universal testing machine and were consistent with the osmotic pressure curve. The inset shows a magnified graph at a high swelling ratio. The blocking stresses of the wrapped gel and the bare gel are marked. The blocking stress of the wrapped gel with a low swelling ratio (1.53) was 1.44 MPa, whereas the osmotic pressure of the bare gel with the same polymer weight was 0.008 MPa. (D) Comparison of turgor pressures between our turgor actuator, plants, and tires.

In the longitudinal (z) direction, the swelling stress is balanced with the blocking stress of the turgor actuator. From Eq. 4, the blocking stress can be expressed as

$$\sigma_{block}^{wrapped} = \sigma_{sw,z} \approx \pi_{os} \quad (6)$$

By having the gel constrained in a membrane, the hydrogel turgor actuator can exploit the high osmotic pressure (π_{os}) of the hydrogel as the blocking stress ($\sigma_{block}^{wrapped}$).

To verify Eq. 6 experimentally, the blocking stresses of the hydrogel turgor actuators were compared with the osmotic pressures in various swelling ratios (Fig. 1C and fig. S2; see methods for details) (21). As shown in Fig. 1C, the blocking stresses are consistent with the osmotic pressure curve (table S1). The actuators achieved a broad range of pressure, up to 1.44 MPa (Fig. 1D).

To evaluate the turgor effect, the actuation stresses and speeds of the bare hydrogel and the turgor actuator were measured as illustrated in Fig. 2A. Poly(3-sulfopropylacrylate) potassium salt (PSPA) polyelectrolyte hydrogels were used for the actuators because the ionizable polymer

chains contribute to high osmotic pressure (see methods and fig. S3 for detailed fabrication of the turgor actuators) (22). As shown in Fig. 2B, the blocking stress of the turgor actuator reaches 0.46 MPa (421 N)—16.8 times as large as that of the bare hydrogel. The actuation speeds of the bare hydrogel and the turgor actuator are both very slow, taking about 4 days to reach the equilibrium swollen state (fig. S4).

We also measured the blocking stresses of the hydrogel turgor actuators with various swelling ratios by changing the initial volume of the hydrogel (V_{gel}) inside the membrane (Fig. 2C). As the inner volume (V_{memb}) of the turgor actuators was the same for each, the gels with larger initial volume swelled less, retaining the higher osmotic pressures and exerting the large blocking stresses. For the same reason, the blocking stress of the actuator increases as the stroke decreases (fig. S5). The maximum stress of the hydrogel turgor actuator is 1.44 MPa (1330 N) with a swelling ratio of 1.53. The maximum stress was obtained immediately before the gel was squeezed out through the pores in the membrane in response to the excessively large

turgor pressure developed inside the membrane (fig. S6).

The strength of the turgor actuator was also substantially higher than that of the bare hydrogel. To demonstrate the strength of the turgor actuators intuitively, dead weights were loaded on a bare hydrogel and a turgor actuator with the same amount of hydrogel (movie S1 and Fig. 2, D and E). Both were fully swollen in deionized water. The bare gel, which had a swelling ratio of 125 (fig. S7 and S8), was completely crushed under 38.4 N of load (Fig. 2D). By contrast, the turgor actuator containing the same hydrogel (swelling ratio of 17.4) in its membrane endured a much heavier weight (184 N) and recovered to its original state when unloaded (Fig. 2E). To quantitatively compare the two actuators in terms of strength, their compressive force-strain curves were measured. As shown in Fig. 2F, a hydrogel turgor actuator endured 917 N of compressive force before the membrane ruptured, which is a value 22 times as large as that of the fully swollen bare hydrogel (41 N). The compressive strength of the turgor actuators was limited by the durability of the wrapping, such as the adhesion strength or the toughness of the membrane.

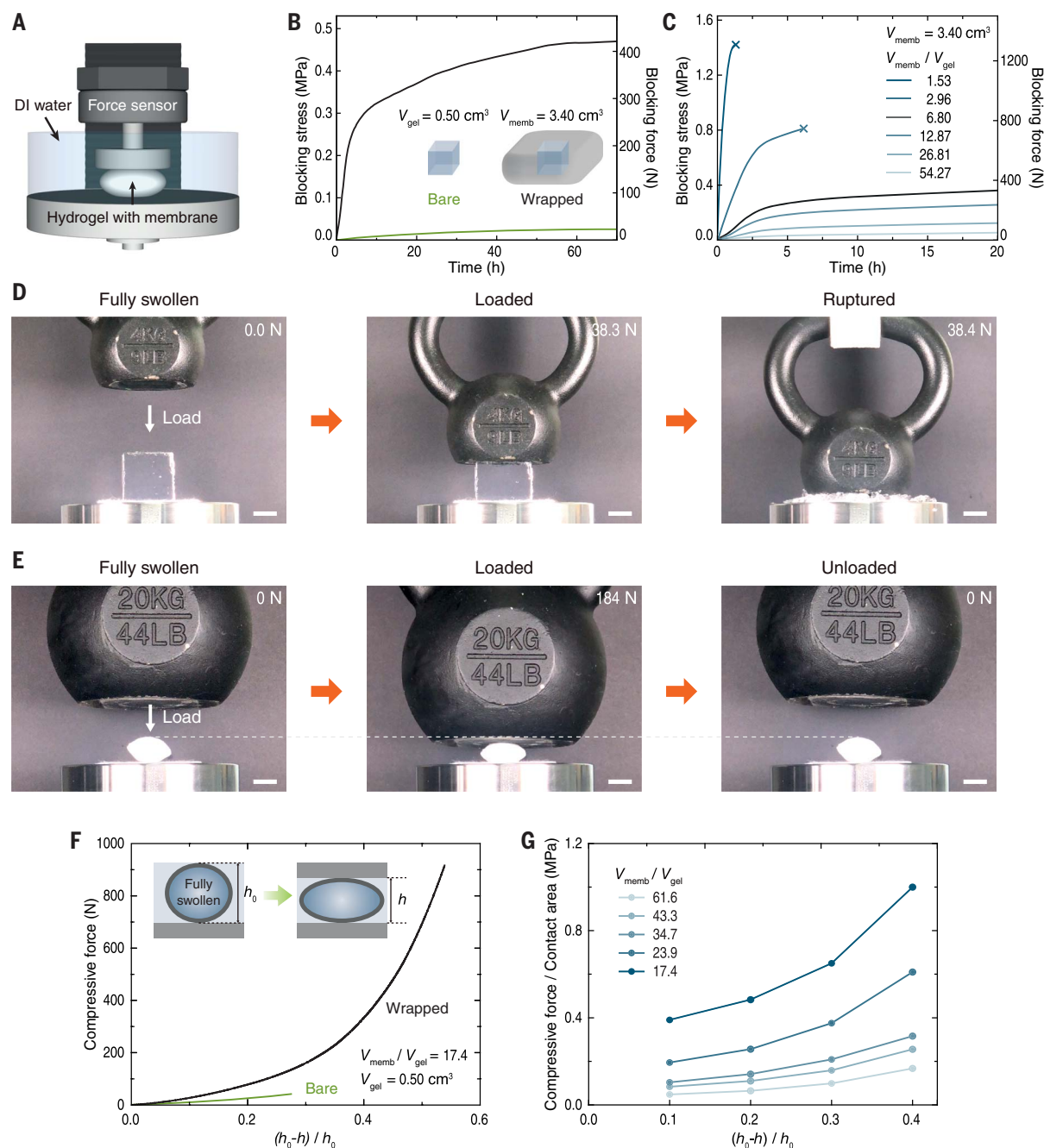


Fig. 2. Mechanical properties of the osmosis-driven hydrogel turgor actuator. **(A)** Schematic illustration of the setup for the constrained swelling experiment. A PSPA hydrogel wrapped in a selectively permeable membrane was placed between two rigid plates with a fixed height. **(B and C)** The stress generated by the turgor actuator was measured as a function of time. **(B)** Wrapped turgor actuator compared with a bare hydrogel. **(C)** Blocking stresses of the turgor actuators with different membrane-to-gel volumetric ratios were investigated. **(D and E)** Compression tests of a fully swollen bare hydrogel **(D)** and a turgor actuator **(E)**. Weights were suspended from a force sensor and slowly lowered at 5 mm/s; 4- and 20-kg kettlebells

were used, respectively. The bare gel ruptured at 38.3 N, whereas the wrapped gel endured 184 N and recovered its original shape when unloaded. Scale bars, 2 cm. **(F)** Compressive force-strain $[(h_0-h)/h_0]$ curves for a bare hydrogel and a wrapped hydrogel with a swelling ratio of 17.4. **(G)** Compressive true stress, (compressive force)/(contact area), versus strain, $(h_0-h)/h_0$, curve for turgor actuators with the swelling ratio of the gel inside the membrane at various strains. The stiffness (tangential slope of compressive stress-strain curve) decreases with the swelling ratio ($V_{\text{memb}}/V_{\text{gel}}$), which is inversely related to the osmotic pressure of the turgor actuators.

To evaluate the effect of the osmotic pressure on the mechanical properties of the turgor actuators, true compressive stress-strain curves were measured at various swelling ratios. Strain is defined as $[(h-h_0)/h_0]$, where

h_0 and h are the heights of the uncompressed and compressed samples, respectively. As shown in Fig. 2G, the true stress at the same strain increases with the osmotic pressure of the hydrogel inside the membrane. Further,

the stiffness of the turgor actuator (tangential slope of the compressive stress-strain curve) increases with the osmotic pressure (see supplementary text). Altogether, the mechanical properties of a turgor actuator can be

manipulated by controlling the swelling ratio of the hydrogel.

Although hydrogel turgor actuators can generate large actuation stress by using the osmotic pressure, actuation speeds are fairly low because the actuations are driven by the diffusion of water. To achieve fast actuation, we added an electroosmotic effect to that of the osmosis. Electroosmosis is a constant and rapid water flow through the electric double layer (EDL) of charged porous materials under an electric field. As illustrated in Fig. 3A, a polyelectrolyte hydrogel contains fixed charges bound to the polymer network, forming an EDL (23). Thus, the counterions in the electrolyte solution can migrate across the charged polymer mesh under an electric field, thereby dragging the water into the gel network (24). The dragged water molecules are captured by the hydrophilic polymer chain, which leads to the swelling of the hydrogel. This active transport of water allows the polyelectrolyte gels to swell much faster than they do in osmosis-driven swelling.

To characterize the electroosmosis-driven actuation of the hydrogel turgor actuator, we measured the blocking stress and speed. As shown in Fig. 3B, the electroosmotic actuation ($V_{\text{memb}}/V_{\text{gel}} = 2.94$, $E = 12$ V/cm) was much faster than the osmosis-driven actuation. The electroosmotic stress generation rate (~ 0.23 MPa/min) was about 22 times as fast as that of the corresponding osmotic rate (~ 0.01 MPa/min) at the initial stage of actuation (30 s). The maximum stress generated by the electroosmotic actuation (~ 0.79 MPa) is similar to that generated by the osmotic actuation (~ 0.73 MPa) with the gel squeezed out through the membrane by the high turgor pressure. However, without squeeze-out of the gel, the actuation stress and speed increased with the electric field intensity (Fig. 3F and table S2). The improvement in actuation stress by electroosmosis was also observed in various strokes (fig. S5). In a stress relaxation test, the maximum and relaxed stresses of the electroosmotic turgor actuator are both much higher than those of the osmotic turgor actuator (fig. S10 and supplementary text). The effects of the cross-linker density, the sign of the charged monomer, and the external solution concentration on the electroosmotic actuation were investigated (fig. S11 and supplementary text). As demonstrated in Fig. 3C, this force generator can break a rigid brick. Under a 4-V/cm electric field, the turgor actuator broke a brick within 5 min (movie S2). The critical stress used to break the brick was ~ 0.38 MPa (570 N) (fig. S12). Further, a turgor actuator composed of a hydrogel with a volume of 4.3 cm³ lifted a 21-kg weight to twice the initial height (fig. S13). From the area under the force-stroke curve (fig. S5) and the slope of the stroke-time curves (fig. S14), the work density and the

power density of the turgor actuator were respectively calculated as 7.0 MJ/m³ and 2.33 kW/m³, thereby outperforming current hydrogels ($\sim 10^{-2}$ kJ/m³ and $\sim 10^{-5}$ kW/m³) (17). Additionally, reversible actuation of the turgor actuator can be achieved by controlling the electric field (fig. S15 and supplementary text).

We theoretically analyzed the kinetics of the electroosmotic actuation of the turgor actuator. Electroresponsive hydrogels have been conventionally used as bending actuators, in which the bending direction was the primary interest. Most previous studies have focused on the interface between the fully swollen hydrogel and the surrounding solution (9, 25, 26). The rate of electroosmotic flow (EOF) in a porous medium (Q_{in}), the pore size of which is much larger than the Debye length, is given by (27)

$$Q_{\text{in}} = \frac{\varepsilon E \zeta \phi A}{\mu} \quad (7)$$

where ε , E , ζ , ϕ , μ , and A are the permittivity of the liquid, an electric field, the zeta potential of the medium, the porosity of the medium, the viscosity of the liquid, and the inlet area, respectively. The electroosmotic inflow (Q_{in}) is either absorbed by the hydrogel (Q_{abs}) or passes through the hydrogel (Q_{out}): $Q_{\text{in}} = Q_{\text{abs}} + Q_{\text{out}}$ (Fig. 3E, inset). In the early stages of the electroosmosis-driven swelling, the entire electroosmotic inflow is absorbed by the gel: $Q_{\text{in}} \approx Q_{\text{abs}}$. This is because water dragged into the hydrogel from the solution by electroosmosis is captured by the hydrophilic polymer network, as shown in fig. S16. When the hydrogel reaches the swelling equilibrium, the EOF merely passes through the hydrogel: $Q_{\text{abs}} \approx 0$.

As shown in Fig. 3D, the mass of the gel increases linearly over time at the initial stage, the slopes of which increase with the electric field intensity. Swelling ceases when a gel is fully swollen. Under an electric field of 1 to 6 V/cm, the average swelling rate until reaching the fully swollen state is 43.5 to 205 times as fast as that of pure osmosis. Fig. 3E shows that the measured swelling rates are consistent with our theory that predicts the linear increase of the swelling rate with the intensity of the electric field (see methods for details). By measuring flow rates through saturated hydrogels, we found that the outlet flow rates (Q_{out}) also increase linearly with the electric field intensity (fig. S17). We also found that the mass of the fully swollen gel by an electric field >2 V/cm is always 150% as large as that by osmosis (fig. S18). This is attributed to the fact that the equilibrium volume of a hydrogel is associated with the stretch limit of a polymer network (28).

We model the actuation stress exerted by the turgor actuators. Under an electric field, a polyelectrolyte gel can absorb the water by both osmosis and electroosmosis. Under osmosis, the osmotic pressure (π_{os}) induces the diffusion of the liquid into the gel, whereas the

membrane pressure resulting from osmosis ($P_{\text{memb,os}}$) squeezes out the liquid. The diffusion flux associated with osmosis (q_{os}) follows Fick's law $q_{\text{os}} = -DcV_{\text{m}}|\nabla P|/(RT)$ where D , c , V_{m} , P , R , and T respectively denote the self-diffusion coefficient of the liquid, the liquid concentration of the polyelectrolyte gel, the molar volume of the liquid, the pressure, the gas constant, and the temperature (29). The pressure driving the diffusion is given by $\Delta P = \pi_{\text{os}} - P_{\text{memb,os}}$, and the diffusion flow rate is written as $Q_{\text{os}} = DcV_{\text{m}}A\Delta P/(\delta RT)$, where A is the liquid inlet area and δ is the ion concentration boundary layer thickness. For the turgor actuator, c and δ are assumed constant because the gel volume is fixed in the relatively stiff membrane. The membrane pressure corresponds to the mechanical stress developed inside the gel that is restrained from swelling, $P_{\text{memb,os}} = K\gamma_0$, with K and γ_0 respectively being the bulk modulus of the polyelectrolyte gel and the restrained volumetric strain due to osmosis (30). Because γ_0 originated from $[Q_{\text{os}}dt/V_0]$, we write $P_{\text{memb,os}} = K[Q_{\text{os}}dt/V_0]$ with V_0 being the volume of the polyelectrolyte gel turgor actuator. By substituting $Q_{\text{os}} = V_0(dP_{\text{memb,os}}/dt)/K$ in Fick's law above and solving, we get

$$P_{\text{memb,os}} = \pi_{\text{os}}(1 - e^{-t/\tau_0}) \quad (8)$$

where $\tau_0 = RTV_0\delta/(DcV_{\text{m}}KA)$.

Under electroosmosis, the electroosmotic pressure drives the liquid flow into the polyelectrolyte gel, whereas the membrane pressure resulting from electroosmosis ($P_{\text{memb,eos}}$) tends to drive the liquid flow out of the gel. The inflow driven by electroosmosis is expressed as Eq. 7. The outflow driven by the membrane pressure follows Darcy's law, $q_e = -(k/\mu)|\nabla P_{\text{memb,eos}}|$, which describes the viscous liquid flux q_e through a porous medium with permeability k . Therefore, the total inlet flow rate is the difference between the electroosmotic inflow rate and the membrane pressure-driven outflow rate: $Q_e = (\varepsilon\zeta E\phi - k\Delta P_{\text{memb,eos}}/L)A/\mu$, where L is the characteristic length of the polyelectrolyte gel. Q_e causes membrane pressure as a result of a volumetric strain $P_{\text{memb,eos}} = K[Q_e dt/V_0]$. Using $Q_e = V_0(dP_{\text{memb,eos}}/dt)/K$, we get

$$P_{\text{memb,eos}} = \eta_e(1 - e^{-t/\tau_e}) \quad (9)$$

where $\eta_e = \varepsilon\zeta E\phi L/k$ and $\tau_e = \mu LV_0/(kKA)$. Therefore, the total membrane pressure $P_{\text{memb}} = P_{\text{memb,os}} + P_{\text{memb,eos}}$ is obtained as

$$P_{\text{memb}} = \pi_{\text{os}}(1 - e^{-t/\tau_0}) + \eta_e(1 - e^{-t/\tau_e}) \quad (10)$$

meaning, as shown in Eqs. 5 and 6, that blocking stress equals the water inflow pressure in the equilibrium state: $\sigma_{\text{block}}^{\text{wrapped}} \approx P_{\text{memb}} \approx \pi_{\text{os}} + \eta_e = P_{\text{in}}$. Finally, the total membrane stress generates

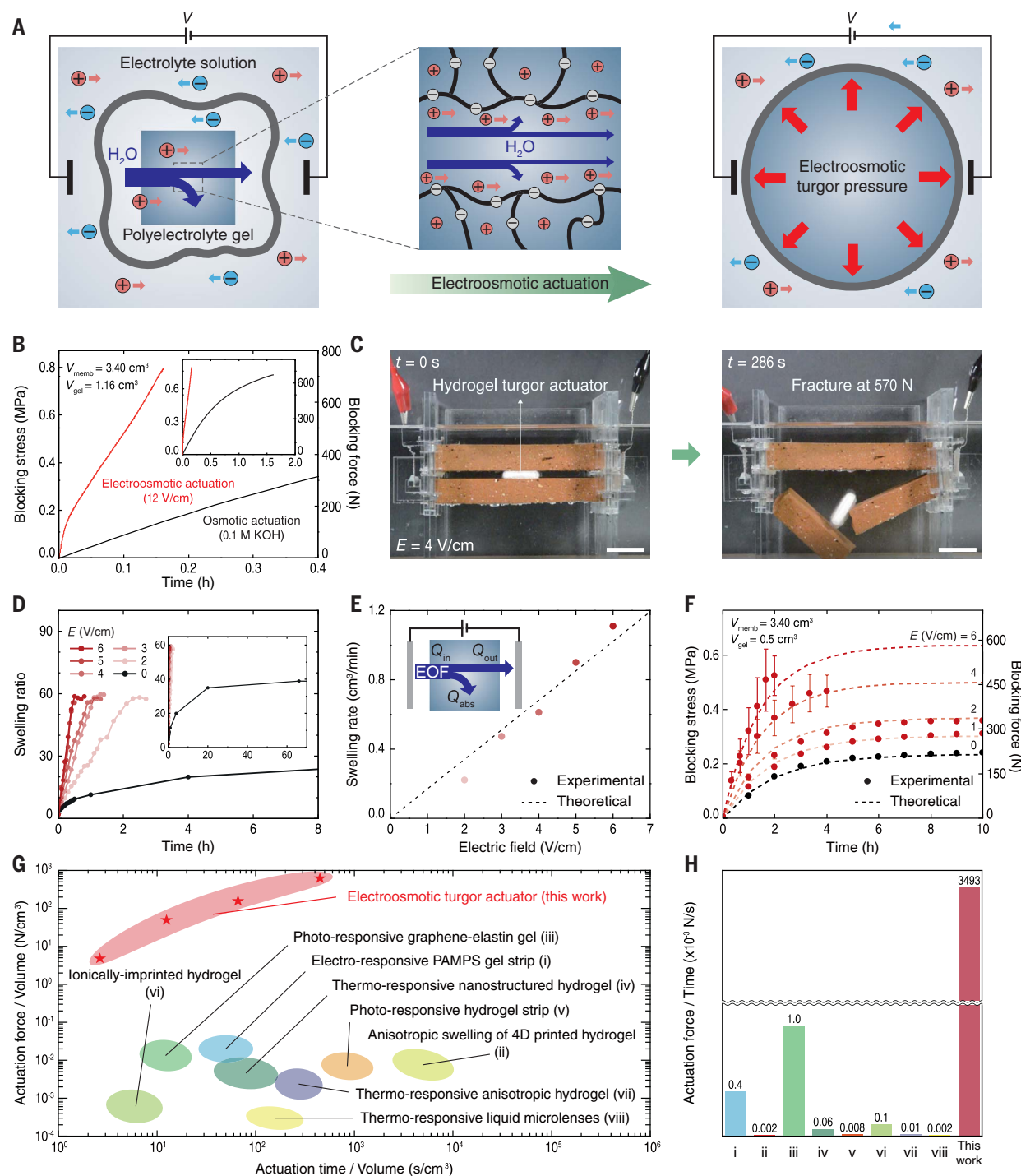


Fig. 3. Electroosmotic actuation of the hydrogel turgor actuator in electrolyte solution. (A) Schematic illustration of the electroosmotic actuation process of a hydrogel turgor actuator in an electrolyte solution. The turgor actuator was placed between platinum electrodes in KOH solution. When a voltage was applied, potassium ions migrated through the negatively charged polymer mesh, causing electroosmotic flow (EOF) inside the gel. The flow caused the gel to swell rapidly, generating a large turgor pressure inside the membrane. (B) Blocking stress versus time curves for the hydrogel turgor actuator actuated by osmosis and electroosmosis at zero stroke. The same turgor actuators ($V_{memb} = 3.40 \text{ cm}^3$, $V_{gel} = 1.16 \text{ cm}^3$) were used for each measurement. The inset shows the stress versus time over a long time scale. (C) Brick breaking within 5 min with turgor actuator operated by electroosmosis with a 4-V/cm electric field. The average stress at the fracture of the brick was $\sim 0.38 \text{ MPa}$ (570 N). Scale bar, 3 cm.

(D) Swelling ratio change of bare hydrogels under different electric field intensities. (E) Electric field dependence of the swelling rate of bare gels with an electroosmotic actuation where $Q_{in} \approx Q_{abs}$. The gel absorbed water at the rate of Q_{abs} as a part of the water inflow rate Q_{in} , whereas the remainder (Q_{out}) flowed out of the gel. (F) Blocking stress of turgor actuator ($V_{memb} = 3.40 \text{ cm}^3$, $V_{gel} = 0.5 \text{ cm}^3$) versus time with different electric field intensities. The dashed line shows the theoretical prediction of the stress evolution of hydrogel turgor actuators. Error bars denote SDs; $N = 3$. (G) Ashby plot of the actuation force and time, which are normalized by volume of the hydrogel, for the electroosmotic turgor actuators and other osmotic actuators. The hydrogel turgor actuators exhibited the largest force and the fastest speed simultaneously. The data used are summarized in table S2. (H) Force generation rates (that is, actuation force divided by corresponding actuation time) of electroosmotic turgor actuators and other osmotic actuators.

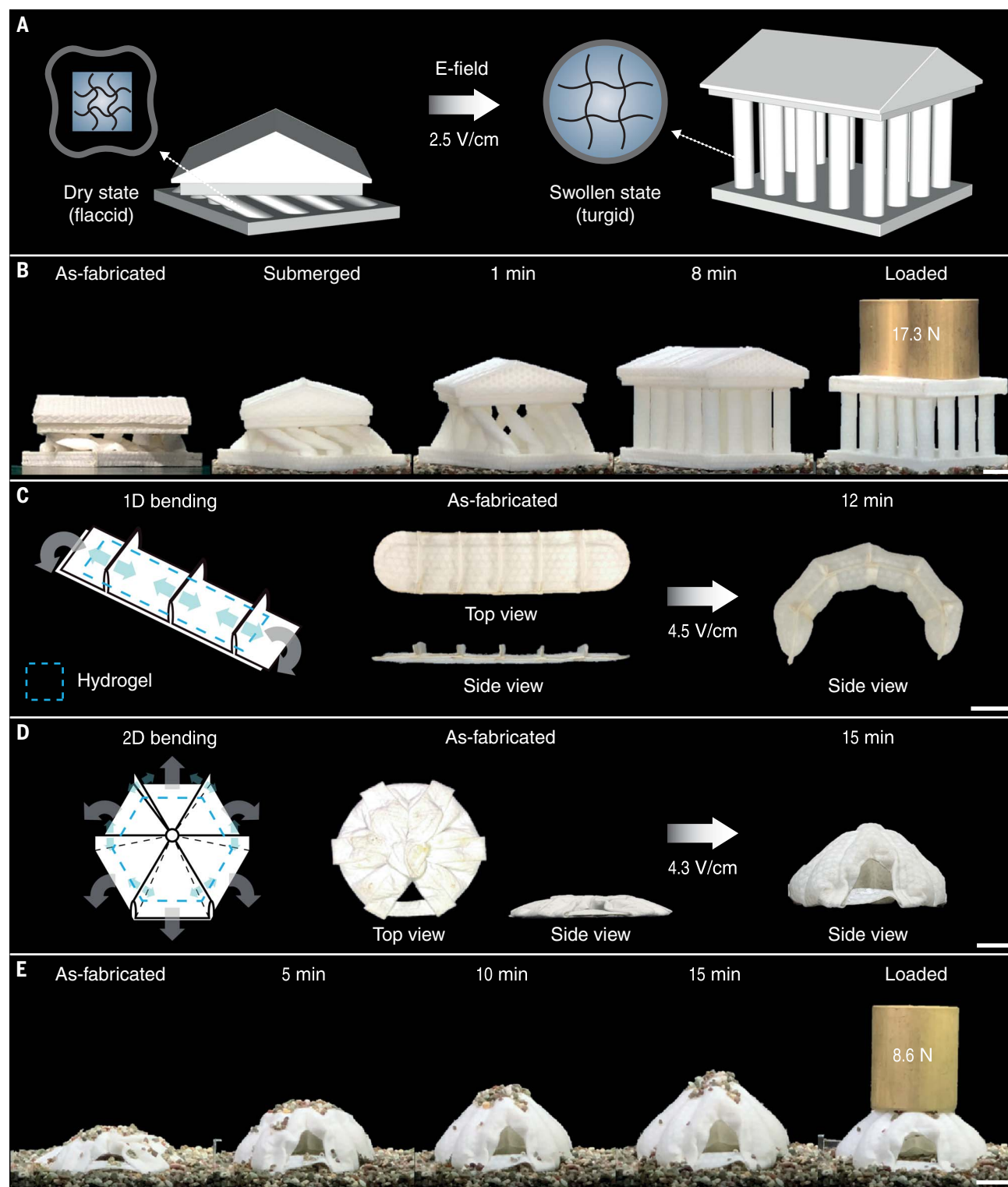


Fig. 4. Rapid construction of underwater structures. (A) Schematic illustrations of the construction of a Greek temple by electroosmotic actuation. The pillars of the Greek temple were initially filled with dry hydrogel and thus started from a fully collapsed structure. Actuation was conducted at 2.5 V/cm in 0.1-M KOH aqueous solution. (B) Rapid construction of the temple with actuation time ~8 min. The completed temple endured two weights measuring 19.6 N, and their effective load is calculated to be 17.3 N by considering the buoyancy. (C) Schematic

illustration and pictures of the 1D bending structure with joints. When the hydrogel swelled, the wrinkles unfolded in the direction of the sky-blue arrow and the system bent in the direction of the gray arrow. The actuation was conducted under a 4.5-V/cm electric field for 12 min. (D) Schematic illustration and pictures of 2D bending resulting in the formation of an igloo. The actuation was conducted under a 4.3-V/cm electric field. (E) Actuation progress for construction of the igloo for 15 min. The complete igloo endured the effective load (8.6 N) considering the buoyancy. Scale bars, 2 cm.

the actuation force of the hydrogel turgor actuator as

$$F = \sigma_{\text{block}}^{\text{wrapped}} A_c \approx P_{\text{memb}} A_c = \pi_{\text{os}} A_c \left(1 - e^{-t/\tau_0}\right) + \eta_c A_c \left(1 - e^{-t/\tau_c}\right) \quad (11)$$

where A_c is the area over which the force is applied.

Using the parameter values obtained from the literature and experiments as described in table S4 and the supplementary text, we calculated the theoretical actuation stress of the turgor actuator and plotted the results (dashed lines) in Fig. 3F. We can see that the calculated actuation stresses are consistent with the experimental data under electric fields ranging from 0 to 6 V/cm. We can also see that the generated blocking stress approached the osmotic pressure of the turgor actuator once the electric field was turned off (fig. S20).

Overall, the electroosmotic turgor actuators exhibited stronger and faster actuations compared to typical osmotic hydrogel actuators (table S5), especially with actuation force increased by a factor of 10^2 to 10^6 (Fig. 3G). The acceleration in swelling by electroosmosis (Fig. 3D), combined with the design employing turgor pressure, leads to substantially faster force generation (3.5 N/s) than that of the osmotic actuator (below 0.001 N/s) (Fig. 3H).

We used the hydrogel turgor actuators as a structural material in an aqueous environment because they can swell rapidly and withstand large forces (movies S3 and S4). We first demonstrated the rapid construction of a Greek temple structure, the columns of which were made of polyelectrolyte gel (Fig. 4A). As shown in Fig. 4B, the columns were flaccid before applying the electric field, so the roof and the floor of the temple were in contact. However, when the electric field of 2.5 V/cm was applied, the columns gradually lifted the roof for ~8 min, thus forming a complete Greek temple structure. This underwater temple endured a 17.3 N of effective load, considering buoyancy.

We further demonstrated the construction of a complicated structure by incorporating wrinkles within the membrane. The wrinkles on the membrane act as joints which unfold when the gel swells inside the membrane. A rod-shaped 1D actuator showed in-plane bending (Fig. 4C), whereas a planar 2D actuator showed out-of-plane bending (Fig. 4D). Two-dimensional bending of the planar actuator led to creation of an igloo-like shelter structure within 15 min of application of a 4.3-V/cm electric field. The underwater igloo endured a weight of 8.6 N, considering buoyancy. Even without an electric field, a turgor actuator can still serve as a support as a result of osmotic pressure. Thus, constructed structures can continually maintain their shape with high stiffness in an aqueous environment.

We proposed a hydrogel-based strong and fast turgor actuator that converts high osmotic pressure into a corresponding strong actuation stress with the aid of a membrane. Electroosmotic actuation makes the turgor actuator substantially faster and stronger by the active transport of water into the hydrogel. The actuators were used to break a rigid brick and build complex underwater structures within a few minutes. Our dynamic model of the actuation is expected to serve as a guideline for the control of a prospective soft robot. Our strategies can be applied to other elastomer- or hydrogel-based actuators, as they provide enhanced mechanical power while retaining the intrinsic advantages of the materials and thereby extend the scope of applications.

REFERENCES AND NOTES

1. Y. Lee *et al.*, *Sci. Robot.* **5**, eaaz5405 (2020).
2. I. Must, E. Sinibaldi, B. Mazzolai, *Nat. Commun.* **10**, 344 (2019).
3. M. Choi *et al.*, *Nat. Photonics* **7**, 987–994 (2013).
4. D. J. Beebe *et al.*, *Nature* **404**, 588–590 (2000).
5. S. Zhang *et al.*, *Nat. Mater.* **14**, 1065–1071 (2015).
6. H. Qin, T. Zhang, N. Li, H. P. Cong, S. H. Yu, *Nat. Commun.* **10**, 2202 (2019).
7. J. Zheng *et al.*, *J. Mater. Chem. C Mater. Opt. Electron. Devices* **6**, 1320–1327 (2018).
8. Z. Han *et al.*, *ACS Appl. Mater. Interfaces* **12**, 12010–12017 (2020).
9. D. Morales, E. Palleau, M. D. Dickey, O. D. Velev, *Soft Matter* **10**, 1337–1348 (2014).

10. S.-L. Xiang, Y.-X. Su, H. Yin, C. Li, M.-Q. Zhu, *Nano Energy* **85**, 105965 (2021).
11. S. Juodkazis *et al.*, *Nature* **408**, 178–181 (2000).
12. L. W. Xia *et al.*, *Nat. Commun.* **4**, 2226 (2013).
13. Z. Jiang, B. Diggle, I. C. G. Shackelford, L. A. Connal, *Adv. Mater.* **31**, e1904956 (2019).
14. Z. Jiang *et al.*, *Chem. Mater.* **33**, 7818–7828 (2021).
15. P. Song, Y. F. Zhang, J. Z. Kuang, *J. Mater. Sci.* **42**, 2775–2781 (2007).
16. Y. S. Kim *et al.*, *Nat. Mater.* **14**, 1002–1007 (2015).
17. Y. Ma *et al.*, *Sci. Adv.* **6**, eabd2520 (2020).
18. H. Yuk *et al.*, *Nat. Commun.* **8**, 14230 (2017).
19. X. Liu, J. Liu, S. Lin, X. Zhao, *Mater. Today* **36**, 102–124 (2020).
20. J. Li, Y. Hu, J. J. Vlassak, Z. Suo, *Soft Matter* **8**, 8121–8128 (2012).
21. W. R. K. Illeperuma, J.-Y. Sun, Z. Suo, J. J. Vlassak, *Soft Matter* **9**, 8504–8511 (2013).
22. J. Li, Z. Suo, J. J. Vlassak, *Soft Matter* **10**, 2582–2590 (2014).
23. X. Zhou, K. Zhao, *Phys. Chem. Chem. Phys.* **19**, 20559–20572 (2017).
24. J. Ko *et al.*, *ACS Nano* **14**, 11906–11918 (2020).
25. M. Doi, M. Matsumoto, Y. Hirose, *Macromolecules* **25**, 5504–5511 (1992).
26. T. Shiga, Y. Hirose, A. Okada, T. Kurauchi, *J. Appl. Polym. Sci.* **46**, 635–640 (1992).
27. R. F. Probstein, "Electroosmosis" in *Physicochemical Hydrodynamics: An Introduction* (Wiley, ed. 2, 1994), pp. 197–202.
28. M. Rubinstein, R. H. Colby, in *Polymer Physics* (Oxford Univ. Press, 2003), pp. 74–78.
29. R. B. Bird, W. E. Stewart, E. N. Lightfoot, *Transport Phenomena* (Wiley, 2006).
30. G. Lin, S. Chang, C.-H. Kuo, J. Magda, F. Solzbacher, *Sens. Actuators B Chem.* **136**, 186–195 (2009).

ACKNOWLEDGMENTS

Funding: This work was supported by National Research Foundation of Korea (NRF) grants funded by the Korean Government (2018M3A7B4089670, 2018-052541, and 2021R1A2C2092737). The Institute of Engineering Research at Seoul National University provided the research facilities for this work. **Author contributions:** H.-Y.K., and J.-Y.S. supervised the research. All authors contributed to interpreting the results and preparing the manuscripts. H.N., Y.-W.K., and C.S.P. conceived the concept, designed the experiments, fabricated the devices, and collected data. S.J. developed the theoretical modeling and performed data analysis. **Competing interests:** The authors declare no competing interests. **Data and materials availability:** All data are available in the main text or supplementary materials.

SUPPLEMENTARY MATERIALS

science.org/doi/10.1126/science.abm7862
Materials and Methods
Supplementary Text
Figs. S1 to S26
Tables S1 and S5
References (31–44)
Movies S1 to S4

12 October 2021; accepted 16 March 2022
10.1126/science.abm7862

Hydrogel-based strong and fast actuators by electroosmotic turgor pressure

Hyeonuk NaYong-Woo KangChang Seo ParkSohyun JungHo-Young KimJeong-Yun Sun

Science, 376 (6590), • DOI: 10.1126/science.abm7862

Wrap it up

Conventional stimuli-responsive hydrogel actuators generally suffer from weak actuation force and slow response speed because of the osmotic-driven actuation mechanism. They are also limited in how much pressure they can endure and will collapse or shatter if pushed too hard. Na *et al.* significantly increased the actuation stress of a hydrogel wrapping the gel in a relatively stiff but flexible semipermeable membrane, which confined the transverse deformation (see the Perspective by Jiang and Song). This effect is similar to the turgor pressure seen in biological cells. The actuation speed can also be enhanced by adding the electrolyte into the water solution and applying an electric field, which reduces the actuation time from hours to minutes. —MSL

View the article online

<https://www.science.org/doi/10.1126/science.abm7862>

Permissions

<https://www.science.org/help/reprints-and-permissions>

Use of this article is subject to the [Terms of service](#)